ORIGINAL PAPER

B-SPLINE-BASED GALERKIN FINITE ELEMENT APPROACH FOR SOLVING THE TIME-FRACTIONAL BURGERS' EQUATION

AMMARA YASIN[1,2], MUHAMMAD KASHIF IQBAL[1], MUHAMMAD ABBAS[3]

Manuscript received: 30.06.2025; Accepted paper: 06.12.2025;
Published online: 30.12.2025.

Abstract. *In this work, the time-fractional Burgers' equation is solved numerically using a Galerkin finite element method with cubic B-splines as trial and test functions. The Burgers' equation serves as a model for various practical phenomena, such as traffic flow, shock wave formation in fluid dynamics, heat conduction in solids, nonlinear acoustics, boundary layer behavior, and specific aspects of plasma physics. The time-fractional derivative is expressed through the Caputo formula, which is capable of handling both singular and non-singular kernels. Cubic B-splines are used as weighting functions to derive the weak formulation of the governing equation. A transformation process links the global and local coordinate systems. The time-fractional derivative is discretized with the standard finite difference formula, while the Crank-Nicolson scheme is applied to discretize the unknown functions. A stability analysis is performed to evaluate the robustness of the scheme and ensure that errors do not amplify over time. The effectiveness of the proposed methodology is evaluated by solving a range of relevant problems, with results presented both graphically and in tabular form.*

Keywords: *Fractional burgers' equation; Cubic B-spline basis function; Galerkin method; Finite element method; Caputo derivatives.*

1. INTRODUCTION

The concept of fractional calculus dates back three centuries. While it boasts a rich history, the practical applications of fractional calculus have recently garnered significant attention. Nonlinear fractional differential equations have become a focal point of numerous studies, given their frequent occurrence in diverse scientific and engineering domains. These equations are prevalent in fields such as plasma physics, electrical networks, control theory of dynamical systems, probability, statistics, acoustics, material science, optical fibers, biology, solid-state physics, chemical kinetics, chemical physics, fluid mechanics, geochemistry, among others. The concepts of dispersion, dissipation, diffusion, reaction, and convection are intricately linked to the phenomena mentioned above, and they can be effectively studied using nonlinear fractional differential equations. Consequently, exploring exact traveling wave solutions for nonlinear fractional differential equations (NLFDEs) holds significant importance in understanding nonlinear tangible events.

[1] Government College University Faisalabad, Department of Mathematics, 38000 Faisalabad, Pakistan.
E-mail: ammarayasin@gcuf.edu.pk; kashifiqbal@gcuf.edu.pk.
[2] University of Agriculture Faisalabad (UAF), Department of Mathematics & Statistics, 38000 Faisalabad, Pakistan. E-mail: ammara.yasin@uaf.edu.pk.
[3] University of Sargodha, Department of Mathematics, 40100 Sargodha, Pakistan.
E-mail: muhammad.abbas@uos.edu.

https://doi.org/10.46939/J.Sci.Arts-25.4-a11

The subject of the nonlinear Burgers' equation has been extensively studied in many different natural science fields [1-3]. The study of nonlinear Burgers' equation, which arises in the setting of wave evolution, including fluid turbulence, shock wave propagation, gas dynamics in granular media, and elastic wave propagation, has received a lot of attention. The Hopf-Cole transformation, which is used analytically to solve the nonlinear Burgers' equation, has helped to shed light on the physical properties of these waves. In the absence of the pressure factor, the model equation has also been referred to as a Navier-Stokes equation version [4].

The physical processes of weakly nonlinear acoustic waves propagating unidirectional in a gas-filled pipe are described by the fractional Burgers' equation [4]. The combined impact of wall friction across the boundary layer results in the fractional derivative. Other models, including shallow-water waves and waves in bubbly liquids, also exhibit the same structure [6]. This paper focuses on analyzing the time-fractional Burgers' equation:

$$ {}_0^C D_t^\alpha u(z,t) + uu_z - \beta u_{zz} = f(z,t), (z,t)\epsilon\Omega, \tag{1}$$

where $\Omega = (z,t)|a < x < b, 0 < t < T, \beta > 0, 0 < a < 1, f(z,t)$ is a given function, the boundary conditions are

$$ u(a,t) = \psi_1(z), u(b,t) = \psi_2(z), t \epsilon [0,T], \tag{2}$$

the initial condition is

$$ u(z,0) = g_0, z\epsilon(a,b) \tag{3}$$

The definition of the Caputo fractional derivative is given below:

$$ {}_0^C D_t^\alpha = \frac{1}{\Gamma(1-\alpha)} \int_0^t \frac{\partial u(z,s)}{\partial s} \frac{ds}{(t-s)^\alpha}, \alpha\epsilon(0,1), \tag{4}$$

in which Γ (.) denotes the gamma function.

In the existing literature, numerous numerical and semi-analytical methods have been developed to solve the nonlinear time-fractional Burgers' equation. These include the Adomian decomposition method (ADM) [7], variational iteration method (VIM) [8], cubic parametric spline (CPS) method [9], quadratic B-spline Galerkin method (QBSGM) [10], cubic trigonometric B-splines method (CTBSM) [11], Legendre Galerkin spectral method (LGSM) [12], Crank Nicolson approach (CNA) [13], finite difference method (FDM) [14], Chebyshev collocation method (CCM) [15], spectral collocation method (SCM) [14], among others. For further insights, Momani [7] explored a non-perturbative analytical solution of the Time Fractional Burgers Equation (TFBE) using the Adomian Decomposition Method (ADM), while Inc [8] solved it using VIM. El-Danaf and Hadhoud [9] obtained the numerical solution of Eq. (1) using the cubic parametric spline approach. Additionally, Esen and Tasbozan [10] employed the quadratic B-spline Galerkin approach, while Yokus and Kaya [17] applied the expansion method based on the Cole-Hopf transformation to derive solutions for the equation. Likewise, Hassani and Naraghirad [18] and Yaseen and Abbas [11] provided the solution using an optimization technique based on CTBSM [11] and generalized polynomials [18]. Alsaedi et al. [19] derived a smooth solution for the time fractional Burgers' equation (TFBE), whereas Li et al. [19] investigated its solution utilizing the Legendre Galerkin spectral method (LGSM) [12] and the Local Discontinuous Galerkin Method (LDGM) [20]. Akram et al. [21] and Majeed et al. [22] solved TFBE numerically using an extended cubic B-spline function. Additionally, Onal and Esen [13], Chen et al. [23],

Yadav and Pandey [14], and Wang [24] approximated the solution using the (CNA) [13], Fourier spectral method [23], Finite Difference Method (FDM) [14], and the separation of variables method [24], respectively. A spectral shifted Legendre collocation approach was proposed by Bhrawy et al. [25] for the space-time fractional Burgers' equation in both temporal and spatial discretization. Safari and Chen [26] employed FDM and the backward substitution method (BSM) to get the time fractional coupled Burgers' equations (TFCBE) solutions. Doha et al. [27] and Albuohimad and Adibi [15] used the Jacobi Gauss Lobatto collocation method (JGLCM) [27] and CCM [15] to build their solutions. Ahmed et al. [15] employed the Laplace-Adomian Decomposition Method (LADM) [28], the Laplace Variational Iteration Method (LVIM) [15], and the Semi-Analytical Computation Method (SCM) [16] to solve TFCBEs. Additionally, Liu and Hou [15] utilized the Generalized Differential Transform Method, while Hussain et al. [29] applied the Meshfree Spectral Method to solve TFCBEs. Zayernouri and Karniadakis introduced fractional spectral and discontinuous spectral element methods for solving fractional partial differential equations (PDEs), particularly the space-fractional Burgers' equation, as discussed in [30].

2. DESCRIPTION OF THE NUMERICAL SCHEME

Let N and M be two positive integers. Define the time step as $\Delta\tau = \frac{\mathrm{T}}{\mathrm{N}}$ and the space step as $h = \frac{b-a}{\mathrm{M}}$. The time points are $t^n = n\tau$ for $0 \le \mathrm{n} \le \mathrm{N}$ and the spatial points are $z_m = mh$ for $0 \le \mathrm{m} \le \mathrm{M}$. Let u_m^n represent the approximate solution at the point (z_m, t^n). The domain $\mathrm{a} \le \mathrm{z} \le \mathrm{b}$ is uniformly divided into M subintervals $[z_m, z_{m+1}]$ each of length h, where $m = 0,1,2,\dots,M-1$ and $a = z_0 < z_1 < \cdots, < z_{m-1} < z_{\mathrm{M}} = b$. The scheme we use to solve Eq. (1) involves approximating the solution $U(z,t)$ to the exact solution $u(z,t)$ in the form given below:

$$\mathrm{U_M(z,t)} = \sum_{\mathrm{m=-1}}^{\mathrm{M+1}} \mathrm{c_m(t)\mathfrak{B}_m(z)}, \tag{5}$$

where the cubic spline basis functions $\mathfrak{B}_{\mathrm{m}}(z)$ are provided by

$$\mathfrak{B}_{\mathrm{m}}(\mathrm{z}) = \frac{1}{\mathrm{h^3}}\begin{cases} (\mathrm{z}-\mathrm{z_{m-2}})^3, \mathrm{z}\epsilon[\mathrm{z_{m-2}},\ z_{m-1}], \\ \mathrm{h^3}+3\mathrm{h^2}(\mathrm{z}-\mathrm{z_{m-1}})+3\mathrm{h}(\mathrm{z}-\mathrm{z_{m-1}})^2-3(\mathrm{z}-\mathrm{z_{m-1}})^3, \mathrm{z}\epsilon[\mathrm{z_{m-1}},\ z_m], \\ \mathrm{h^3}+3\mathrm{h^2}(\mathrm{z_{m+1}}-\mathrm{z})+3\mathrm{h}(\mathrm{z_{m+1}}-\mathrm{z})^2-3(\mathrm{z_{m+1}}-\mathrm{z})^3, \mathrm{z}\epsilon[\mathrm{z_m},\ z_{m+1}], \\ (\mathrm{z_{m+2}}-\mathrm{z})^3, \mathrm{z}\epsilon[\mathrm{z_{m+1}},\ z_{m+2}], \\ 0, \mathrm{otherwise}. \end{cases}$$

and $c_m(t)$ are unknown functions that need to be found.

Each cubic B-spline function spans four elements, effectively covering the interval $[z_m, z_{m+1}]$ with four such functions. Here, the element knots z_m and z_{m+1}, along with the interval $[z_m, z_{m+1}]$, are utilized to define the finite elements. The determination of the parameter $c_m(t)$ involves utilizing the nodal values $U_{\mathrm{M}}(z_m), U'_{\mathrm{M}}(z_m), U''_{\mathrm{M}}(z_m)$.

$$\begin{aligned} U_M = U(z_m) &= c_{m-1} + 4\,c_m + c_{m+1}, \\ U'_{\mathrm{M}} = U'(z_m) &= \frac{3}{h}(c_{m+1} - c_{m-1}), \\ U''_{\mathrm{M}} = U''(z_m) &= \frac{6}{h^2}(c_{m-1} - 2c_m + c_{m+1}). \end{aligned} \tag{6}$$

Within the standard element $[z_m,\ z_{m+1}]$, the change of $U_{\mathrm{M}}\ (z,t)$ is given by

$$U_M(z,t) = \sum_{j=m-1}^{m+2} c_j(t)\ \mathfrak{B}_j\ (z) \tag{7}$$

The temporal Caputo derivative can be approximated using the L1 formula.

$$\frac{\partial^\alpha u}{\partial \mathrm{t}^\alpha} = \frac{(\Delta \mathrm{r})^{-\alpha}}{\Gamma(2-\alpha)} \sum_{k=0}^{n-1} ((k+1)^{1-\alpha} - k^{1-\alpha}\ )(u^{n-k+1} - u^{n-k}). \tag{8}$$

Using (8) along with the $\theta-$ weighted method, Eq. (1) can be rewritten as:

$$\begin{aligned} \frac{(\Delta \mathrm{r})^{-\alpha}}{\Gamma(2-\alpha)} \sum_{k=0}^{n-1} ((k+1)^{1-\alpha} - k^{1-\alpha}\ )(u^{n-k+1} - u^{n-k}) + \theta(u^{n+1}u_z^{n+1} - \beta u_{zz}^{n+1}) \\ + (1-\theta)(u^n u_z^n - \beta u_{zz}^n) = f(z, t^{n+1}). \end{aligned} \tag{9}$$

By [26], linearize the non-linear term as

$$(uu_z)^{n+1} = u_z^{n+1}u^n + u_z^n u^{n+1} - u_z^n u^n.$$

Discretizing (9) for $\theta = \frac{1}{2}$, we achieve

$$\begin{aligned} &\frac{1}{2}\ (u_z^{n+1}u^n + u_z^n u^{n+1}) - \frac{\beta}{2}(u_{zz}^{n+1}) \\ &= \frac{\beta}{2}(u_{zz}^n) - \eta \sum_{k=0}^{n-1} p^k (u^{n-k+1} - u^{n-k}) + f^{n+1}, \end{aligned} \tag{10}$$

where, $\eta = \frac{(\Delta \mathrm{r})^{-\alpha}}{\Gamma(2-\alpha)}$, $p^k = ((k+1)^{1-\alpha} - k^{1-\alpha})$.

By applying the Galerkin method to Eq. (10) with weight functions $\mathbb{W}$, we obtain the following integral equation

$$\begin{aligned} &\frac{1}{2}\int_a^b (u_z^{n+1}u^n + u_z^n u^{n+1} - \beta u_{zz}^{n+1})\ \mathbb{W} dz \\ &= \frac{\beta}{2}\int_a^b u_{zz}^n\ \mathbb{W} dz - \eta \int_a^b \sum_{k=0}^{n-1} p^k (u^{n-k+1} - u^{n-k})\ \mathbb{W} dz \\ &+ \int_a^b f^{n+1}\ \mathbb{W} dz\ . \end{aligned} \tag{11}$$

Since the integrand includes first and second derivatives, it is necessary to choose trial functions that are at least cubic polynomials. By employing cubic B-splines as trial functions in the Galerkin finite element method, we can achieve smooth solutions of first and second order respectively. The interval $[z_m,\ z_{m+1}]$, is transformed into $[0, h]$ via local coordinates, where $\mathrm{r} = z - z_m$, $0 \le \mathrm{r} \le h$ and $0 \le \mathrm{r} \le h$. The cubic B-spline shape functions, in terms of r over $[0, h]$, can be written as

$$\begin{aligned}\mathfrak{B}_{\mathrm{m}-1} &= \left(1-\frac{\mathfrak{r}}{h}\right)^3,\\ \mathfrak{B}_{\mathrm{m}} &= 4-3\frac{\mathfrak{r}}{h}+3\left(1-\frac{\mathfrak{r}}{h}\right)^2-3\left(1-\frac{\mathfrak{r}}{h}\right)^3, 0\le \mathfrak{r}\le h\\ \mathfrak{B}_{\mathrm{m}+1} &= 1+3\frac{\mathfrak{r}}{h}+3\left(\frac{\mathfrak{r}}{h}\right)^2-3\left(\frac{\mathfrak{r}}{h}\right)^3,\\ \mathfrak{B}_{\mathrm{m}+2} &= \left(\frac{\mathfrak{r}}{h}\right)^3.\end{aligned} \tag{12}$$

As a finite element $[z_m,\ z_{m+1}]$, is spanned by four consecutive cubic B-splines, the local approximation over the element is given by:

$$U_{\mathrm{M}}^{e} = \mathfrak{B}_{\mathrm{m}-1}(\mathfrak{r})c_{m-1}(t)+\mathfrak{B}_{\mathrm{m}}(\mathfrak{r})c_m(t)+\mathfrak{B}_{\mathrm{m}+1}(\mathfrak{r})c_{m+1}(t)+\mathfrak{B}_{\mathrm{m}+2}(\mathfrak{r})c_{m+2}(t) \tag{13}$$

Here, $c^e=(c_{m-1},\ c_m,\ c_{m+1},c_{m+2})$ represent the element parameters, and $\mathfrak{B}^{\mathrm{e}}=(\mathfrak{B}_{\mathrm{m}-1},\mathfrak{B}_{\mathrm{m}},\mathfrak{B}_{\mathrm{m}+1},\mathfrak{B}_{\mathrm{m}+2})$ denote the element cubic B-spline shape functions. By substituting $\mathbb{W}$ and U with the weight functions $\mathfrak{B}$ and the trail solution (13), respectively, into Eq. (11), we obtain the following matrix system of first-order ordinary differential equations.

$$\begin{aligned}\sum_{j=m-1}^{m+2}\left[\left(\eta\int_0^h \mathfrak{B}_\ell\mathfrak{B}_{\mathrm{j}}d\mathfrak{r}+\frac{\eta_1}{2}\int_0^h \mathfrak{B}_\ell\mathfrak{B}_j'd\mathfrak{r}+\frac{\eta_2}{2}\int_0^h \mathfrak{B}_\ell\mathfrak{B}_{\mathrm{j}}d\mathfrak{r}+\frac{\beta}{2}\int_0^h \mathfrak{B}_\ell'\mathfrak{B}_j'd\mathfrak{r}\right)\left(c_j^e\right)^{n+1}\right]\\ = \beta\sum_{j=m-1}^{m+2}\left(\mathfrak{B}_\ell\mathfrak{B}_j'\right)|_0^h\left(c_j^e\right)^n-\frac{\beta}{2}\left(\int_0^h \mathfrak{B}_\ell'\mathfrak{B}_j'd\mathfrak{r}\right)\left(c_j^e\right)^n\\ -\eta\sum_{j=m-1}^{m+2}\left(\int_0^h \mathfrak{B}_\ell\mathfrak{B}_{\mathrm{j}}d\mathfrak{r}\right)\sum_{k=1}^{n-1}p^k\left(c_j^{n-k+1}-c_j^{n-k}\right)+\int_0^h \mathfrak{B}_{\mathrm{l}}f_1(\mathfrak{r},t)d\mathfrak{r}\end{aligned} \tag{14}$$

where $l=m-1,m,m+1,m+2$ and $m=0,1,\dots,M-1.\eta_1=U^n$ and $\eta_2=U_z^n$ are assumed constant within the element to simplify the calculation of the integral. If we define the element matrices by:

$$\begin{aligned}\mathrm{A}_{\ell\mathrm{j}}=\int_0^h \mathfrak{B}_\ell\mathfrak{B}_{\mathrm{j}}d\mathfrak{r},\mathrm{B}_{\ell\mathrm{j}}=\int_0^h \mathfrak{B}_\ell'\mathfrak{B}_j'd\mathfrak{r},\mathrm{L}_{\ell\mathrm{j}}=\int_0^h \mathfrak{B}_\ell\mathfrak{B}_j'd\mathfrak{r},\mathrm{C}_{\ell\mathrm{j}}=\mathfrak{B}_\ell\mathfrak{B}_j'|_0^h,E_\ell\\ =\int_0^h \mathfrak{B}_{\mathrm{l}}f_1(\mathfrak{r},t)d\mathfrak{r}\end{aligned} \tag{15}$$

The aggregation of elemental contributions yields the following matrix equation:

$$\begin{aligned}\left(\left(\eta+\frac{\eta_2}{2}\right)\mathrm{A}+\frac{\eta_1}{2}\mathrm{L}+\frac{\beta}{2}\mathrm{B}\right)\mathrm{c}^{n+1}\\ =\beta C\mathrm{c}^n-\frac{\beta}{2}\beta\mathrm{c}^n-\eta\mathrm{A}\sum_{k=1}^{n-1}p^k\left(c_j^{n-k+1}-c_j^{n-k}\right)+E\end{aligned} \tag{16}$$

where $c^n=(c_{-1}^n,c_0^n,\dots c_{\mathrm{M}}^n,c_{\mathrm{M}+1}^n)^{\mathrm{T}}$ contain all the element parameters. The assembled matrices A, B, C and L are septadiagonal. Applying boundary conditions (2) eliminates c_{-1}^n and $c_{\mathrm{M}+1}^n$ from system (16), resulting in a $(M+1)\times(M+1)$ system solvable by a modified Thomas algorithm. The time evolution of nodal values $c^{n+1}$is obtained iteratively

after determining the initial vector c^0. We use the following approximation for this initial condition.

$$U_{\mathrm{M}}(z,0)=\sum_{\mathrm{m}=-1}^{M+1} c_m^0(t)\ \mathfrak{B}_{\mathrm{m}}\ (z).$$

The following relationships must hold at the points z_m to ensure U_M is satisfied:

$$U_{\mathrm{M}}(z_m,0)=u(z_m,0), for\ m=0,1,\ldots \mathrm{M}.$$

The initial vector c^0can be computed using the initial and boundary conditions through the following matrix equations.

$$\begin{bmatrix} 4 & 1 & 0 & 0 & & & 0 \\ 1 & 4 & 1 & 0 & & & \\ 0 & 1 & 4 & 1 & & & \\ & \ddots & \ddots & \ddots & & & \\ & & 1 & 4 & 1 & & \\ & & 0 & 1 & 4 & 1 & \\ 0 & & & 0 & 1 & 4 & \end{bmatrix}\begin{bmatrix} c_0^0 \\ c_1^0 \\ c_2^0 \\ \vdots \\ c_{\mathrm{M}-2}^0 \\ c_{\mathrm{M}-1}^0 \\ c_{\mathrm{M}}^0 \end{bmatrix}=\begin{bmatrix} g_0(x_0)+\frac{h}{3}g_0'(x_0) \\ g_0(x_1) \\ g_0(x_2) \\ \vdots \\ g_0(x_{\mathrm{M}-2}) \\ g_0(x_{\mathrm{M}-1}) \\ g_0(x_{\mathrm{M}})+\frac{h}{3}g_0'(x_{\mathrm{M}}) \end{bmatrix}$$

3. STABILITY ANALYSIS

The notion of stability is intrinsically linked to the control of computational errors [22]. In this section, the stability of the proposed method is analyzed using the Fourier approach, as outlined in [8]. For every Fourier mode, an amplification factor is derived, which describes how the amplitude of a specific mode changes from one time step to the next in the numerical solution. This factor evaluates the extent to which errors at a specific wavenumber propagate across successive iterations. The numerical scheme is deemed stable if the magnitude of the amplification factor does not exceed 1 for all wavenumbers. To verify the stability of the proposed numerical scheme (16), it is sufficient to analyze the homogeneous case, $f(z,t)$, of Eq. (1). The process begins by introducing a recurrence relationship that ties the unknown element parameters across consecutive time levels, as outlined below

$$\begin{gathered}\left(\frac{h}{140}\left(\eta+\frac{\eta_2}{2}\right)-\frac{\eta_1}{40}-\frac{3\beta}{20\mathrm{h}}\right)c_{m-3}^{n+1}+\left(\frac{120\mathrm{h}}{140}\left(\eta+\frac{\eta_2}{2}\right)-\frac{56\eta_1}{40}-\frac{72\beta}{20\mathrm{h}}\right)c_{m-2}^{n+1}+\\ \left(\frac{1191h}{140}\left(\eta+\frac{\eta_2}{2}\right)-\frac{245\eta_1}{40}-\frac{45\beta}{20\mathrm{h}}\right)c_{m-1}^{n+1}+\left(\frac{2416h}{140}\left(\eta+\frac{\eta_2}{2}\right)+\frac{240\beta}{10\mathrm{h}}\right)c_m^{n+1}+\\ \left(\frac{1191h}{140}\left(\eta+\frac{\eta_2}{2}\right)+\frac{245\eta_1}{40}-\frac{45\beta}{10\mathrm{h}}\right)c_{m+1}^{n+1}+\left(\frac{120h}{140}\left(\eta+\frac{\eta_2}{2}\right)+\frac{56\eta_1}{40}-\frac{72\beta}{10\mathrm{h}}\right)c_{m+2}^{n+1}+\\ \left(\frac{h}{140}\left(\eta+\frac{\eta_2}{2}\right)+\frac{\eta_1}{40}-\frac{3\beta}{10\mathrm{h}}\right)c_{m+3}^{n+1}=\frac{\beta}{2}\left(\frac{3}{10\mathrm{h}}c_{m-3}^{n}+\frac{72}{10\mathrm{h}}c_{m-2}^{n}+\frac{45}{10\mathrm{h}}c_{m-1}^{n}-\right.\\ \left.\frac{240}{10\mathrm{h}}c_m^n+\frac{45}{10\mathrm{h}}c_{m+1}^n+\frac{72}{10\mathrm{h}}c_{m+2}^n+\frac{3}{10\mathrm{h}}c_{m+3}^n\right)-\eta\frac{h}{140}\left[\sum_{k=1}^{n}p^k\left(c_{m-3}^{n-k+1}-c_{m-3}^{n-k}\right)+\right.\\ 120\left(c_{m-2}^{n-k+1}-c_{m-2}^{n-k}\right)+1191\left(c_{m-1}^{n-k+1}-c_{m-1}^{n-k}\right)+2416\left(c_m^{n-k+1}-c_m^{n-k}\right)+\\ \left.1191\left(c_{m+1}^{n-k+1}-c_{m+1}^{n-k}\right)+120\left(c_{m+2}^{n-k+1}-c_{m+2}^{n-k}\right)+\left(c_{m+3}^{n-k+1}-c_{m+3}^{n-k}\right)\right].\end{gathered}\tag{17}$$

Let $\mathcal{V}$ and $\tilde{\mathcal{V}}$ represent the growth factor and its approximation, respectively, for a Fourier mode. By defining $\Upsilon_m^n=\mathcal{V}-\tilde{\mathcal{V}}$ and substituting it into Eq. (17), we obtain:

$$\left(\frac{h}{140}\left(\eta+\frac{\eta_2}{2}\right)-\frac{\eta_1}{40}-\frac{3\beta}{20\mathrm{h}}\right)\Upsilon_{m-3}^{n+1}+\left(\frac{120\mathrm{h}}{140}\left(\eta+\frac{\eta_2}{2}\right)-\frac{56\eta_1}{40}-\frac{72\beta}{20\mathrm{h}}\right)\Upsilon_{m-2}^{n+1}+\left(\frac{1191h}{140}\left(\eta+\frac{\eta_2}{2}\right)-\frac{245\eta_1}{40}-\frac{45\beta}{20\mathrm{h}}\right)\Upsilon_{m-1}^{n+1}+\left(\frac{2416h}{140}\left(\eta+\frac{\eta_2}{2}\right)+\frac{240\beta}{10\mathrm{h}}\right)\Upsilon_{m}^{n+1}+\left(\frac{1191h}{140}\left(\eta+\frac{\eta_2}{2}\right)+\frac{245\eta_1}{40}-\frac{45\beta}{10\mathrm{h}}\right)\Upsilon_{m+1}^{n+1}+\left(\frac{120h}{140}\left(\eta+\frac{\eta_2}{2}\right)+\frac{56\eta_1}{40}-\frac{72\beta}{10\mathrm{h}}\right)\Upsilon_{m+2}^{n+1}+\left(\frac{h}{140}\left(\eta+\frac{\eta_2}{2}\right)+\frac{\eta_1}{40}-\frac{3\beta}{10\mathrm{h}}\right)\Upsilon_{m+3}^{n+1}=\frac{\beta}{2}\left(\frac{3}{10\mathrm{h}}\Upsilon_{m-3}^{n}+\frac{72}{10\mathrm{h}}\Upsilon_{m-2}^{n}+\frac{45}{10\mathrm{h}}\Upsilon_{m-1}^{n}-\frac{240}{10\mathrm{h}}\Upsilon_{m}^{n}+\frac{45}{10\mathrm{h}}\Upsilon_{m+1}^{n}+\frac{72}{10\mathrm{h}}\Upsilon_{m+2}^{n}+\frac{3}{10\mathrm{h}}\Upsilon_{m+3}^{n}\right)-\eta\frac{h}{140}\left[\sum_{k=1}^{n}p^{k}\left(\Upsilon_{m-3}^{n-k+1}-\Upsilon_{m-3}^{n-k}\right)+120\left(\Upsilon_{m-2}^{n-k+1}-\Upsilon_{m-2}^{n-k}\right)+1191\left(\Upsilon_{m-1}^{n-k+1}-\Upsilon_{m-1}^{n-k}\right)+2416\left(\Upsilon_{m}^{n-k+1}-\Upsilon_{m}^{n-k}\right)+1191\left(\Upsilon_{m+1}^{n-k+1}-\Upsilon_{m+1}^{n-k}\right)+120\left(\Upsilon_{m+2}^{n-k+1}-\Upsilon_{m+2}^{n-k}\right)+\left(\Upsilon_{m+3}^{n-k+1}-\Upsilon_{m+3}^{n-k}\right)\right]. \tag{18}$$

The aforementioned error equation adheres to the given initial and boundary conditions

$$\Upsilon_m^0=g_0(z_m),m=0,1,2,\dots,\mathrm{M}, \tag{19}$$

$$\Upsilon_0^{\mathrm{n}}=\phi_1(t^n),\Upsilon_{\mathrm{M}}^{\mathrm{n}}=\phi_1(t^n). \tag{20}$$

Define the grid function

$$\Upsilon^{\mathrm{n}}=\begin{cases}\Upsilon_m^{\mathrm{n}},z_m-\dfrac{h}{2}<z<z_m+\dfrac{h}{2},m=1{:}\,1{:}\,\mathrm{M}-1,\\ 0,\mathrm{a}\le\mathrm{z}\le\mathrm{a}+\dfrac{\mathrm{h}}{2}\ or\ b-\dfrac{h}{2}\le\mathrm{z}\le\mathrm{b}.\end{cases} \tag{21}$$

The Fourier expansion of $\Upsilon^{\mathrm{n}}(z)$ is defined as

$$\Upsilon^{\mathrm{n}}(z)=\sum_{g=-\infty}^{\infty}\Lambda^n(\mathrm{g})\exp^{\frac{2\pi\mathrm{IZG}}{b-a}},\mathrm{n}=1,2,\dots.\mathrm{N}, \tag{22}$$

where

$$\Lambda^n(g)=\frac{1}{b-a}\int_a^b\mu^n(z)exp^{\frac{2\pi\imath zg}{b-a}}dz. \tag{23}$$

Let

$$\Upsilon^{\mathrm{n}}=[\Upsilon_1^n,\Upsilon_2^n,\dots,\Upsilon_{\mathrm{M}-1}^n]^{\mathrm{T}},$$

and consider the norm defined by

$$\|\Upsilon^{\mathrm{n}}\|_2=\left(\sum_{m=1}^{\mathrm{M}-1}h|\Upsilon_m^n|^2\right)^{\frac{1}{2}}=\left[\int_a^b|\Upsilon_m^n|^2dz\right]^{\frac{1}{2}}.$$

Using Parseval's equality, we obtain

$$\int_a^b|\Upsilon^n|^2dz=\sum_{g=-\infty}^{\infty}|\Lambda^n(\mathrm{g})|^2,$$

which implies that

$$\|\boldsymbol{\Upsilon^{\mathrm{n}}}\|_{\mathbf{2}}^{\mathbf{2}}=\sum_{\boldsymbol{g}=-\infty}^{\infty}|\boldsymbol{\Lambda^n(\mathrm{g})}|^{\mathbf{2}}. \tag{24}$$

Suppose the solutions to Eqs. $(18-20)$, takes the form $\Upsilon^{n}=\varsigma^{n}exp^{\iota\gamma m\theta}$, with $\iota=\sqrt{-1}\ and\ \gamma\epsilon|-\pi,\pi|$. Substituting this into Eq. (18) and dividing by $exp^{\iota\gamma m\theta}$ yields.

$$\begin{gathered}\varsigma^{n+1}[(\mathcal{K}_1-\mathcal{K}_2)cos3\theta\Upsilon+(120\mathcal{K}_1-24\mathcal{K}_2)(cos2\theta\Upsilon)+\\(1191\mathcal{K}_1-15\mathcal{K}_2)(cos\theta\Upsilon)+(2416\mathcal{K}_1+80\mathcal{K}_2)+\iota(\mathcal{K}_3sin3\theta\Upsilon+56\sin2\theta\Upsilon+\\245\sin\theta\Upsilon)]=\varsigma^{n}[\mathcal{K}_2cos3\theta\Upsilon+24\mathcal{K}_2cos2\theta\Upsilon+15\mathcal{K}_2cos\theta\Upsilon-80\mathcal{K}_{12}]-\\\eta\frac{h}{140}\left[\sum_{k=1}^{n}p^{k}\,(\varsigma^{n-k+1}-\varsigma^{n-k})\big((2cos3\theta\Upsilon)+120(2cos2\theta\Upsilon)+1191(2cos\theta\Upsilon)+\\2416\big)\right],\end{gathered}\tag{25}$$

where $\mathcal{K}_1=\frac{h}{70}\left(\eta+\frac{\eta_2}{2}\right),\mathcal{K}_2=\frac{3\beta}{10\mathrm{h}}\ ,\mathcal{K}_3=\frac{\eta_1}{20}$. Without any loss of generality, let $\Upsilon=0$. This reduces the last expression to

$$\varsigma^{n+1}=\frac{\mathcal{V}_1}{\mathcal{V}}\varsigma^{n}-\frac{\mathcal{V}\mathcal{V}_2}{\mathcal{V}_1}\sum_{k=1}^{n}p^{k}\,(\varsigma^{n-k+1}-\varsigma^{n-k}),\tag{26}$$

where $\mathcal{V}=3728\mathcal{K}_1+30\mathcal{K}_2,\ \mathcal{V}_1=-30\mathcal{K}_2,\ \mathcal{V}_2=\frac{3728\eta h}{70}$.

Now we have to show that

$$|\varsigma^{n}|\le|\varsigma^{0}|,n=1,2,\dots,\mathrm{N}.\tag{27}$$

We will prove this result using mathematical induction. For the case $n=0$, Eq. (26() yields

$$|\varsigma^{1}|=\frac{\mathcal{V}_1}{\mathcal{V}}|\varsigma^{0}|\le|\varsigma^{0}|,since\ \frac{\mathcal{V}_1}{\mathcal{V}}<1.\tag{28}$$

Suppose that $|\varsigma^{n}|\le|\varsigma^{0}|$ for $n=0,1,2,\dots N-1$. We have to prove it for $n=j+1$. Now consider

$$\begin{aligned}|\varsigma^{n+1}|&=\left|\tfrac{\mathcal{V}_1}{\mathcal{V}}\varsigma^{\mathrm{n}}-\tfrac{\mathcal{V}\mathcal{V}_2}{\mathcal{V}_1}\textstyle\sum_{k=1}^{n}p^{k}\,(\varsigma^{n-k+1}-\varsigma^{n-k})\right|,\\&\le\left|\tfrac{\mathcal{V}_1}{\mathcal{V}}\varsigma^{\mathrm{n}}\right|+\left|\tfrac{\mathcal{V}\mathcal{V}_2}{\mathcal{V}_1}\textstyle\sum_{k=1}^{n}p^{k}\,(\varsigma^{n-k+1}-\varsigma^{n-k})\right|,\\&\le\left|\tfrac{\mathcal{V}_1}{\mathcal{V}}\varsigma^{\mathrm{n}}\right|+\tfrac{\mathcal{V}\mathcal{V}_2}{\mathcal{V}_1}\textstyle\sum_{k=1}^{n}p^{k}\,|(\varsigma^{n-k+1}-\varsigma^{n-k})|,\\&\le\tfrac{\mathcal{V}_1}{\mathcal{V}}|\varsigma^{\mathrm{n}}|+\tfrac{\mathcal{V}\mathcal{V}_2}{\mathcal{V}_1}\textstyle\sum_{k=1}^{n}\ |\varsigma^{n-k+1}|+|\varsigma^{n-k}|,\\&\le\tfrac{\mathcal{V}_1}{\mathcal{V}}|\varsigma^{0}|+\tfrac{\mathcal{V}\mathcal{V}_2}{\mathcal{V}_1}\textstyle\sum_{k=1}^{n}\ |\varsigma^{0}|+|\varsigma^{0}|,\\&=\tfrac{\mathcal{V}_1}{\mathcal{V}}|\varsigma^{0}|+\tfrac{2n\mathcal{V}\mathcal{V}_2}{\mathcal{V}_1}|\varsigma^{0}|,\\&=\frac{\mathcal{V}_1^{2}+2n\mathcal{V}^{2}\mathcal{V}_2}{\mathcal{V}\mathcal{V}_1}|\varsigma^{0}|.\end{aligned}$$

Hence

$$|\varsigma^{n+1}|\le|\varsigma^{0}|,\text{if}\ \frac{\mathcal{V}_1^{2}+2n\mathcal{V}^{2}\mathcal{V}_2}{\mathcal{V}\mathcal{V}_1}<1.\tag{29}$$

From Eq. (24) and (29), it follows that

$$\|\Upsilon_m^{\mathrm{n}}\|_2\le\ \|\Upsilon_m^{0}\|_2,n=0,1,2,\dots,\mathrm{N}.$$

It follows that the numerical scheme exhibits conditional stability.

4. NUMERICAL EXAMPLE AND RESULTS

In this section, three numerical examples are examined to evaluate the effectiveness and precision of the proposed method. The results are compared with both existing methods from the literature and exact solutions. These comparisons are made across various nodal points z_m at specific time levels t^n, using a defined mesh size h and time step $\Delta\mathbf{r}$. The numerical simulations were carried out in Mathematica 12. To assess the precision of the proposed method, the maximum and Euclidean error norms were calculated using the formulas below

$$\mathfrak{L}_\infty = max_{1\le m\le \mathrm{M}+1}|u(z,t) - \mathrm{U}(z,t)|\,,$$
$$\mathfrak{L}_2 = h\sum_{m=1}^{\mathrm{M}+1}|u(z,t) - \mathrm{U}(z,t)|^2.$$

Example 1. We consider the one-dimensional time-fractional burger equation with $a \in (0,1]$. [19].

$$_0^cD_t^\alpha\, u(z,t) + uu_z\, - \beta u_{zz} = f(z,t), 0 \le \mathrm{z} \le 1, \mathrm{t} \ge 0,$$

where,

$$f(z,t) = \frac{2t^{2-\alpha}e^z}{\Gamma(3-\alpha)} + t^4e^{2z} - t^2e^z.$$

With the following conditions

$$u(z,0) = 0,$$
$$u(0,\mathrm{t}) = t^2, \mathrm{u}(1,t) = et^2.$$

The exact solution of the problem is given as follows

$$u(z,t) = t^2e^z.$$

Table 1 presents numerical solutions for $\alpha = 0.5, \mathrm{M} = 40, \mathrm{T} = 0.05$, considering various Δt values. As evident from Table 1, both $\mathfrak{L}_\infty$ and $\mathfrak{L}_2$ error norms decrease as $\Delta\mathbf{r}$ diminishes, aligning with expectations. Table 1 also presents a comparison of results obtained using the method developed in this paper with those reported in [19]. The results indicate that the proposed method outperforms the method presented in [19]. Table 2 displays numerical solutions for different α values under the conditions $\Delta\mathbf{r} = 0.00025, M = 40, T = 0.05$. The results demonstrate a negative correlation between α and both $\mathfrak{L}_\infty$ and $\mathfrak{L}_2$ error norms. Table 3 presents $\mathfrak{L}_\infty$ and $\mathfrak{L}_2$ error norms calculated at different spatial nodes for $h = \Delta\mathbf{r}$ and a constant fractional order $\alpha = 0.50$. Error norms for various time intervals are tabulated in Table 4. The performance of the current scheme is showcased through 3D visualizations of both computational and analytical results, depicted in Figs. 1 and 2. Fig. 3 reveals a close alignment between the numerical results obtained using the proposed scheme and the exact outcomes across various time levels. The piece-wise defined spline solution for Example (1) is presented when $T = 0.05, h = 0.01$, and $\Delta\mathbf{r} = 0.01$.

$$U(z,0.05)$$

$$=\begin{cases}
416.66(-4(0.01-\mathrm{z})^3+(0.02-\mathrm{z})^3)+412.503(0.01-\mathrm{z})^3 \\
+425.098(0.+\mathrm{z})^3+420.858(-4(0.+\mathrm{z})^3+(0.01+\mathrm{z})^3), \text{if z}\epsilon\left[0,\frac{1}{100}\right] \\
420.858(-4(0.02-\mathrm{z})^3+(0.03-\mathrm{z})^3)+416.66(0.02-\mathrm{z})^3 \\
+429.38(-0.01+\mathrm{z})^3+425.098(-4(-0.01+\mathrm{z})^3+(0.+\mathrm{z})^3), \text{if z}\epsilon\left[\frac{1}{100},\frac{2}{100}\right] \\
425.098(-4(0.03-\mathrm{z})^3+(0.04-\mathrm{z})^3)+429.38(-4(-0.02+\mathrm{z})^3 \\
+(-0.01+\mathrm{z})^3)+420.858(0.03-\mathrm{z})^3+433.706(-0.02+\mathrm{z})^3, \text{if z}\epsilon\left[\frac{2}{100},\frac{3}{100}\right] \\
429.38(-4(0.04-\mathrm{z})^3+(0.05-\mathrm{z})^3)+433.706(-4(-0.03+\mathrm{z})^3 \\
+(-0.02+\mathrm{z})^3)+425.098(0.04-\mathrm{z})^3+438.074(-0.03+\mathrm{z})^3, \text{if z}\epsilon\left[\frac{3}{100},\frac{4}{100}\right] \\
433.706(-4(0.05-\mathrm{z})^3+(0.06-\mathrm{z})^3)+438.074(-4(-0.04+\mathrm{z})^3 \\
+(-0.03+\mathrm{z})^3)+429.38(0.05-\mathrm{z})^3+442.486(-0.04+\mathrm{z})^3, \text{if z}\epsilon\left[\frac{4}{100},\frac{5}{100}\right] \\
\vdots \qquad \vdots\vdots \\
660.344(-4(0.47-\mathrm{z})^3+(0.48-\mathrm{z})^3)+666.981(-4(-0.46+\mathrm{z})^3 \\
+(-0.45+\mathrm{z})^3)+653.774(0.47-\mathrm{z})^3+673.684(-0.46+\mathrm{z})^3, \text{if z}\epsilon\left[\frac{47}{100},\frac{48}{100}\right] \\
666.981(-4(0.48-\mathrm{z})^3+(0.49-\mathrm{z})^3)+673.684(-4(-0.47+\mathrm{z})^3 \\
+(-0.46+\mathrm{z})^3)+660.344(0.48-\mathrm{z})^3+680.454(-0.47+\mathrm{z})^3, \text{if z}\epsilon\left[\frac{48}{100},\frac{49}{100}\right] \\
673.684(-4(0.49-\mathrm{z})^3+(0.5-\mathrm{z})^3)+680.454(-4(-0.48+\mathrm{z})^3 \\
+(-0.47+\mathrm{z})^3)+666.981(0.49-\mathrm{z})^3+687.292(-0.48+\mathrm{z})^3, \text{if z}\epsilon\left[\frac{49}{100},\frac{50}{100}\right] \\
\vdots \qquad \vdots\vdots \\
1077.46(-4(0.96-\mathrm{z})^3+(0.97-\mathrm{z})^3)+1088.27(-4(-0.95+\mathrm{z})^3 \\
+(-0.94+\mathrm{z})^3)+1066.76(0.96-\mathrm{z})^3+1099.19(-0.95+\mathrm{z})^3, \text{if z}\epsilon\left[\frac{95}{100},\frac{96}{100}\right] \\
1088.27(-4(0.97-\mathrm{z})^3+(0.98-\mathrm{z})^3)+1099.19(-4(-0.96+\mathrm{z})^3 \\
+(-0.95+\mathrm{z})^3)+1077.46(0.97-\mathrm{z})^3+1110.22(-0.96+\mathrm{z})^3, \text{if z}\epsilon\left[\frac{96}{100},\frac{97}{100}\right] \\
1099.19(-4(0.98-\mathrm{z})^3+(0.99-\mathrm{z})^3)+1110.22(-4(-0.97+\mathrm{z})^3 \\
+(-0.96+\mathrm{z})^3)+1088.27(0.98-\mathrm{z})^3+1121.35(-0.97+\mathrm{z})^3, \text{if z}\epsilon\left[\frac{97}{100},\frac{98}{100}\right] \\
1110.22(-4(0.99-\mathrm{z})^3+(1.-\mathrm{z})^3)+1121.35(-4(-0.98+\mathrm{z})^3 \\
+(-0.97+\mathrm{z})^3)+1099.19(0.99-\mathrm{z})^3+1132.6(-0.98+\mathrm{z})^3, \text{if z}\epsilon\left[\frac{98}{100},\frac{99}{100}\right] \\
1121.35(-4(1.-\mathrm{z})^3+(1.01-\mathrm{z})^3)+1132.6(-4(-0.99+\mathrm{z})^3 \\
+(-0.98+\mathrm{z})^3)+1110.22(1.-\mathrm{z})^3+1143.96(-0.99+\mathrm{z})^3, \text{if z}\epsilon\left[\frac{99}{100},\frac{100}{100}\right]
\end{cases}$$

Table 1. Error norms and numerical solutions of Example 1 when $T = 0.05, M = 40$ and $\alpha = 0.50$.

z	$\Delta r = 0.005$	$\Delta r = 0.001$	$\Delta r = 0.0005$	$\Delta r = 0.00025$	*Exact Solution*
0.0	0.0025	0.0025	0.0025	0.0025	0.0025
0.1	0.00277109	0.002764024	0.00276355	0.00276338	0.00276293
0.2	0.00306831	0.00305549	0.00305464	0.00305434	0.00305351
0.3	0.0033946	0.00337735	0.00337621	0.0033758	0.00337465
0.4	0.00375315	0.00373281	0.00373145	0.00373097	0.00372956
0.5	0.0041474	0.00412538	0.00412392	0.0041234	0.0041218
0.6	0.00458105	0.00455897	0.00455751	0.00455699	0.0045553
0.7	0.00505815	0.00503786	0.00503651	0.00503603	0.00503438
0.8	0.00558306	0.00556674	0.00556566	0.00556527	0.00556385
0.9	0.00616053	0.0061508	0.00615015	0.00614992	0.00614901
1.0	0.0067957	0.0067957	0.0067957	0.0067957	0.0067957
$\mathfrak{L}_2$	1.90426×10^{-5}	2.70129×10^{-6}	1.6182×10^{-6}	1.23211×10^{-6}	
$\mathfrak{L}_2$[19]	6.59999×10^{-4}	3.74901×10^{-4}	2.32591×10^{-4}	9.2489×10^{-5}	
$\mathfrak{L}_\infty$	2.5921×10^{-5}	3.67827×10^{-6}	2.21184×10^{-6}	1.69297×10^{-6}	
$\mathfrak{L}_\infty$[19]	9.36512×10^{-4}	5.29997×10^{-4}	3.26112×10^{-4}	1.32945×10^{-4}	

Table 2. Approximate, exact solutions and error norms obtained for different fractional order of Example 1 at $T = 0.05, M = 40, \Delta r = 0.00025$.

z	$\alpha = 0.10$	$\alpha = 0.25$	$\alpha = 0.75$	$\alpha = 0.90$	*Exact Solution*
0.0	0.0025	0.0025	0.0025	0.0025	0.0025
0.1	0.00276246	0.00276185	0.00275918	0.00276018	0.00276293
0.2	0.00305268	0.00305157	0.00304686	0.00304872	0.00305351
0.3	0.00337357	0.00337208	0.0033658	0.00336835	0.00337465
0.4	0.00372835	0.00372658	0.00371917	0.00372218	0.00372956
0.5	0.00412056	0.00411865	0.00411051	0.00411371	0.00412181
0.6	0.00455413	0.00455222	0.00454384	0.00454694	0.0045553
0.7	0.00503339	0.00503164	0.00502366	0.00502638	0.00503438
0.8	0.00556313	0.00556173	0.00555504	0.00555709	0.00556385
0.9	0.00614862	0.00614779	0.00614362	0.00614476	0.00614901
1.0	0.0067957	0.0067957	0.0067957	0.0067957	0.0067957
$\mathfrak{L}_2$	8.97773×10^{-7}	2.30759×10^{-6}	8.51671×10^{-6}	6.22665×10^{-6}	
$\mathfrak{L}_\infty$	1.24242×10^{-6}	3.1555×10^{-6}	1.14973×10^{-5}	8.3527×10^{-6}	

Table 3. The error norms for $\alpha = 0.50, T = 0.05$ of Example 1.

z	$N = M = 50$	$N = M = 100$	$N = M = 200$	$N = M = 400$	*Exact Solution*
0.0	0.0025	0.0025	0.0025	0.0025	0.0025
0.1	0.00275226	0.00275764	0.0027604	0.00276181	0.00276293
0.2	0.00303428	0.00304399	0.00304897	0.00305151	0.00305351
0.3	0.00334885	0.00336189	0.00336858	0.00337198	0.00337465
0.4	0.00369918	0.00371456	0.00372245	0.00372646	0.00372956
0.5	0.00408895	0.00410561	0.00411415	0.00411851	0.00412181
0.6	0.00452231	0.00453907	0.00454767	0.00455205	0.0045553
0.7	0.00500399	0.00501948	0.00502742	0.00503147	0.00503438
0.8	0.00553931	0.00555186	0.00555829	0.00556157	0.00556385
0.9	0.0061343	0.00614185	0.00614572	0.00614769	0.00614901
1.0	0.0067957	0.0067957	0.0067957	0.0067957	0.0067957
$\mathfrak{L}_2$	2.44609×10^{-5}	1.20401×10^{-5}	5.66903×10^{-6}	2.42550×10^{-6}	
$\mathfrak{L}_\infty$	3.32402×10^{-5}	1.63665×10^{-5}	7.71156×10^{-6}	3.30869×10^{-6}	

Table 4. Error norms for various t values with $M = 40$ of Example 1 at $\alpha = 0.50$.

t	$\mathfrak{L}_\infty$	$\mathfrak{L}_2$
0.01	2.24453×10^{-7}	1.66843×10^{-7}
0.03	1.38917×10^{-6}	1.0244×10^{-6}
0.05	2.42438×10^{-6}	1.77327×10^{-6}
0.07	1.57981×10^{-6}	1.04456×10^{-6}
0.09	5.62131×10^{-6}	3.74189×10^{-6}

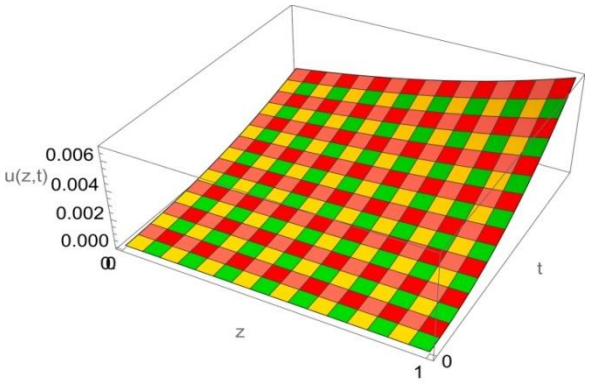

Figure 1. The three-dimensional view of the exact solutions for Example 1 is presented, with $M = 100, \Delta r = 0.01, and\ \alpha = 0.50$.

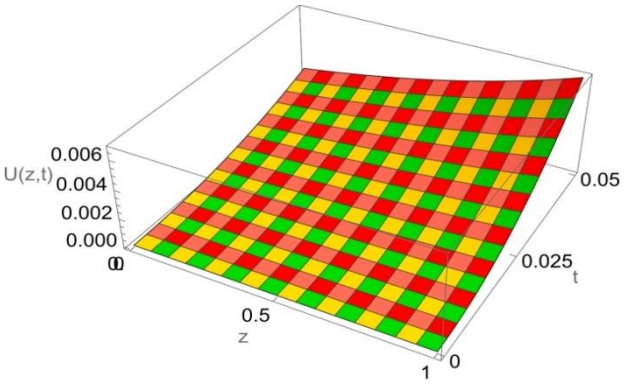

Figure 2. The three-dimensional view of the numerical solutions for Example 1 is presented, when $M = 100, \Delta r = 0.01, and\ \alpha = 0.5$.

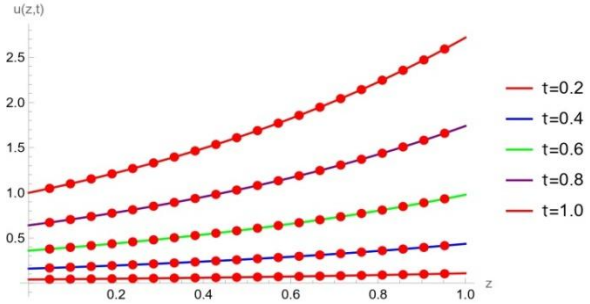

Figure 3. The figure illustrates the numerical and exact solutions for, $M = 100, \Delta r = 0.01, and\ \alpha = 0.5$ across different time stages.

Example 2. We consider the one-dimensional time-fractional burger equation with $\alpha \in (0, 1]$ [19]

$$ {}_0^C D_t^{\alpha}\, u(z,t) + uu_z - \beta u_{zz} = f(z,t), 0 \le z \le 1, t \ge 0, $$

where

$$ f(z,t) = \frac{2t^{2-\alpha} sin(2\pi z)}{\Gamma(3-\alpha)} + 2\pi t^4 sin(2\pi z) cos(2\pi z) - 4\pi^2 t^2 sin(2\pi z). $$

With the following conditions

$$ u(z,0) = 0, $$
$$ u(0,t) = 0, u(1,t) = 0. $$

The exact solution of the problem is given as follows

$$ u(z,t) = t^2 sin(2\pi z). $$

Table (5) demonstrates that the $\mathfrak{L}_\infty$ and $\mathfrak{L}_2$error norms decrease as the time step Δr is reduced, under the conditions $N = 80, T = 0.05, and = 0.50$. For different values of the fractional order α, Table (6) presents both exact and computational results, using the parameters $M = 120, \alpha = 0.5, and\ \Delta r = 0.00255$, evaluated at specific spatial points. The robustness of the scheme is demonstrated through 3D plots of computational and analytical results, as displayed in Figure (4). The numerical results obtained using the proposed method exhibit a high degree of agreement with the exact results at various time levels, as shown in Figure (5). The piece-wise defined spline solution for Example (2) is presented when $T = 1, h = 0.01, and\ \Delta r = 0.01$.

$$U(z,1)$$

$$= \begin{cases} 6.17388\times10^{-15} + z(6.71752 + (-0.000121617 - 46.9656z)z), \text{if } z\epsilon\left[0,\frac{1}{100}\right] \\ -2.52737\times10^{-7} + z(6.71759 + (-0.00770373 - 46.7128z)z), \text{if } z\epsilon\left[\frac{1}{100},\frac{2}{100}\right] \\ -4.41628\times10^{-6} + z(6.71822 + (-0.0389303 - 46.1924z)z), \text{if } z\epsilon\left[\frac{2}{100},\frac{3}{100}\right] \\ -0.0000252054 + z(6.7203 + (-0.108227 - 45.4224z)z), \text{if } z\epsilon\left[\frac{3}{100},\frac{4}{100}\right] \\ -0.0000903782 + z(6.72518 + (-0.230426 - 44.4041z)z), \text{if } z\epsilon\left[\frac{4}{100},\frac{5}{100}\right] \\ \vdots \qquad \vdots\vdots \\ -1.26835 + z\big(19.685 + z(-50.3053 + 33.0893z)\big), \text{if } z\epsilon\left[\frac{47}{100},\frac{48}{100}\right] \\ -1.28298 + z(19.7764 + z(-50.4958 + 33.2216z)), \text{if } z\epsilon\left[\frac{48}{100},\frac{49}{100}\right] \\ -1.29198 + z\big(19.8315 + z(-50.6083 + 33.2981z)\big), \text{if } z\epsilon\left[\frac{49}{100},\frac{50}{100}\right] \\ \vdots \qquad \vdots\vdots \\ 37.3791 + z(-123.675 + (129.329 - 43.0333z)z), \text{if } z\epsilon\left[\frac{95}{100},\frac{96}{100}\right] \\ 38.2753 + z(-126.475 + (132.246 - 44.0461z)z), \text{if } z\epsilon\left[\frac{96}{100},\frac{97}{100}\right] \\ 38.9743 + z(-128.637 + (134.475 - 44.812z)z), \text{if } z\epsilon\left[\frac{97}{100},\frac{98}{100}\right] \\ 39.4615 + z(-130.129 + (135.997 - 45.3297z)z), \text{if } z\epsilon\left[\frac{98}{100},\frac{99}{100}\right] \\ 39.7055 + z(-130.868 + (136.743 - 45.5811z)z), \text{if } z\epsilon\left[\frac{99}{100},\frac{100}{100}\right] \end{cases}$$

Table 5. Error norms and numerical solutions of Example 2 when $T = 0.05, M = 80$ and $\alpha = 0.50$.

z	$\Delta r = 0.005$	$\Delta r = 0.001$	$\Delta r = 0.0005$	$\Delta r = 0.00025$	*Exact Solution*
0.0	0.0000	0.0000	0.0000	0.0000	0.0000
0.1	0.00145473	0.00146637	0.00146794	0.00146875	0.00276293
0.2	0.00235369	0.00237253	0.00237507	0.00237637	0.00305351
0.3	0.00235355	0.00237239	0.00237493	0.00237624	0.00337465
0.4	0.00145451	0.00146615	0.00146772	0.00146853	0.00372956
0.5	−0.0000000	−0.0000000	−0.0000000	−0.0000000	0.00412182
0.6	−0.00145451	−0.00146615	−0.00146772	−0.00146853	0.00455531
0.7	−0.00235355	−0.00237239	−0.00237493	−0.00237624	0.00503438
0.8	−0.00235369	−0.00237253	−0.00237507	−0.00237637	0.00556385
0.9	−0.00145473	−0.00146637	−0. 00146794	−0.00146875	0.00614901
1.0	−0.0000000	−0.0000000	−0.0000000	−0.0000000	−0.0000000
$\mathfrak{L}_2$	1.78593×10^{-5}	3.85331×10^{-6}	1.96262×10^{-6}	9.96297×10^{-6}	
$\mathfrak{L}_2$[19]	1.24034×10^{-4}	5.4081×10^{-5}	1.4255×10^{-5}	1.960×10^{-5}	
$\mathfrak{L}_\infty$	2.52566×10^{-5}	5.44968×10^{-6}	2.78289×10^{-6}	1.42307×10^{-6}	
$\mathfrak{L}_\infty$[19]	1.75611×10^{-4}	7.7465×10^{-5}	2.8523×10^{-5}	4.168×10^{-5}	

Table 6. Approximate, exact solutions and error norms obtained for different fractional order of Example 2 at $\mathbf{T = 0.05, M = 120, \Delta r = 0.00025}$.

z	$\alpha = 0.25$	$\alpha = 0.5$	$\alpha = 0.75$	*Exact Solution*
0.0	0.01	0.01	0.01	0.01
0.1	0.00146918	0.00146875	0.00146818	0.00951057
0.2	0.00237706	0.00237637	0.00237546	0.00809017
0.3	0.00237692	0.00237624	0.00237534	0.00587785
0.4	0.00146894	0.00146853	0.00146798	0.00309017
0.5	0.0000000	0.0000000	0.0000000	0.0000000
0.6	-0.00146894	-0.00146853	-0.00146798	-0.00309017
0.7	-0.00237692	-0.00237624	-0.00237534	-0.00587785
0.8	-0.00237706	-0.00237637	-0.00237546	-0.00809017
0.9	-0.00146918	-0.00146875	-0.00146818	-0.00951057
1.0	0.0000000	0.0000000	0.0000000	0.0000000
$\mathfrak{L}_2$	4.9335×10^{-7}	9.96373×10^{-7}	1.66734×10^{-6}	
$\mathfrak{L}_\infty$	7.25022×10^{-7}	1.42318×10^{-6}	2.36464×10^{-6}	

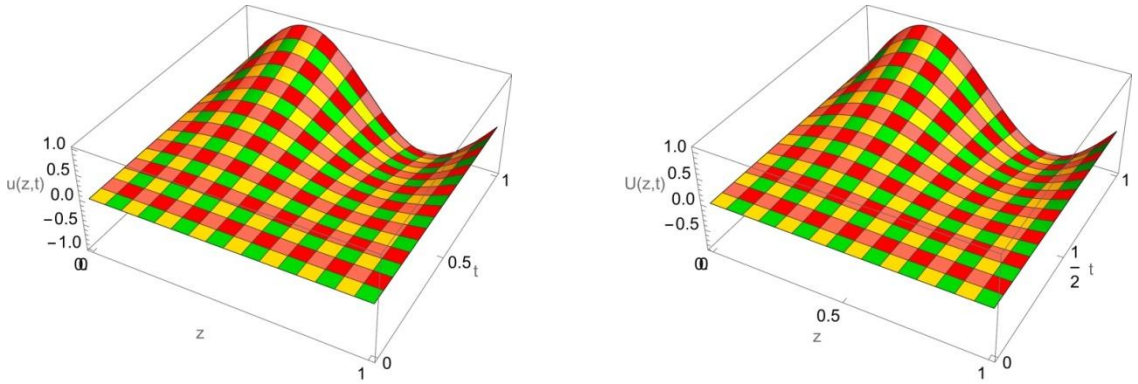

Figure 4. A 3D graphical representation of the exact and approximate solutions for Example 2.

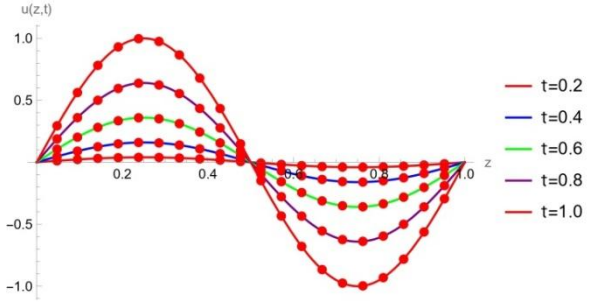

Figure 5. A graph comparing numerical and exact results for $\boldsymbol{M = 100, \Delta r = 0.01}$ *and* $\boldsymbol{\alpha = 0.5}$ at various time levels for Example 2.

Example 3. We consider the one-dimensional time-fractional burger equation with $\boldsymbol{\alpha} \in (\mathbf{0}, \mathbf{1}]$)

$$ {}_0^C D_t^\alpha \, u(z,t) + uu_z - \beta u_{zz} = f(z,t), 0 \le z \le 1, t \ge 0, $$

where,

$$ f(z,t) = \frac{2t^{2-\alpha} cos(\pi z)}{\Gamma(3-\alpha)} - \pi t^4 sin(\pi z) cos(\pi z) + \beta \pi^2 t^2 cos(\pi z). $$

With the following conditions

$$ u(z,0) = 0, $$
$$ u(0,t) = t^2, u(1,t) = -t^2. $$

The exact solution of the problem is given as follows

$$u(z,t) = t^2 cos(\pi z).$$

Table (7) presents the error norms and corresponding numerical results for various $\boldsymbol{\alpha}$ values. Table (8) shows the error norms for $\alpha = 0.9$ at different time stages, and Table (9) presents the error norms in the temporal direction. Figure (6) and Figure (7) demonstrate a strong alignment between the 3D plots of computational and exact solutions for the parameters $T = 0.1, h = 0.0125, and\ \Delta\mathrm{r} = 0.0005$. Meanwhile, Figure (8) presents a comparison of exact and approximate solutions under the same conditions $T = 0.1, h = 0.0125, and\ \Delta\mathrm{r} = 0.0005$ at different time levels. This figure highlights notable variations in the solution profiles as time progresses, illustrating a clear increasing trend between the time levels and the solution behavior. The piece-wise defined spline solution for Example (3) is presented when $T = 0.1, h = 0.0125, and\ \Delta\mathrm{r} = 0.0005$.

$$U(z,0.1) = \begin{cases} 0.01 + \mathrm{z}(-0.0000547955 + (-0.0492676 + 0.00113003\mathrm{z})\mathrm{z}), \text{if } \mathrm{z}\epsilon\left[0, \frac{1}{80}\right] \\ 0.01 + \mathrm{z}(-0.0000538397 + (-0.0493441 + 0.00316909\mathrm{z})\mathrm{z}), \text{if } \mathrm{z}\epsilon\left[\frac{1}{80}, \frac{2}{80}\right] \\ 0.00999996 + \mathrm{z}(-0.0000500723 + (-0.0494948 + 0.00517835\mathrm{z})\mathrm{z}), \text{if } \mathrm{z}\epsilon\left[\frac{2}{80}, \frac{3}{80}\right] \\ 0.00999986 + \mathrm{z}(-0.0000415739 + (-0.0497214 + 0.0071928\mathrm{z})\mathrm{z}), \text{if } \mathrm{z}\epsilon\left[\frac{3}{80}, \frac{4}{80}\right] \\ 0.00999961 + \mathrm{z}(-0.0000265995 + (-0.0500209 + 0.00918937\mathrm{z})\mathrm{z}), \text{if } \mathrm{z}\epsilon\left[\frac{4}{80}, \frac{5}{80}\right] \\ \vdots \qquad \vdots\vdots \\ 0.00964814 + \mathrm{z}(0.00512975 + (-0.0734787 + 0.0492591\mathrm{z})\mathrm{z}), \text{if } \mathrm{z}\epsilon\left[\frac{47}{80}, \frac{48}{80}\right] \\ 0.009782 + \mathrm{z}(0.00446043 + (-0.0723632 + 0.0486393\mathrm{z})\mathrm{z}), \text{if } \mathrm{z}\epsilon\left[\frac{48}{80}, \frac{49}{80}\right] \\ 0.00994155 + \mathrm{z}(0.00367897 + (-0.0710874 + 0.047945\mathrm{z})\mathrm{z}), \text{if } \mathrm{z}\epsilon\left[\frac{49}{80}, \frac{50}{80}\right] \\ \vdots \qquad \vdots\vdots \\ 0.0308585 + \mathrm{z}(-0.0725003 + (0.0224528 + 0.00918935\mathrm{z})\mathrm{z}), \text{if } \mathrm{z}\epsilon\left[\frac{75}{80}, \frac{76}{80}\right] \\ 0.0325703 + \mathrm{z}(-0.0779059 + (0.0281429 + 0.00719282\mathrm{z})\mathrm{z}), \text{if } \mathrm{z}\epsilon\left[\frac{76}{80}, \frac{77}{80}\right] \\ 0.0343665 + \mathrm{z}(-0.0835046 + (0.0339598 + 0.00517833\mathrm{z})\mathrm{z}), \text{if } \mathrm{z}\epsilon\left[\frac{77}{80}, \frac{78}{80}\right] \\ 0.0362288 + \mathrm{z}(-0.0892346 + (0.0398367 + 0.00316911\mathrm{z})\mathrm{z}), \text{if } \mathrm{z}\epsilon\left[\frac{78}{80}, \frac{79}{80}\right] \\ 0.0381924 + \mathrm{z}(-0.0952 + (0.0458776 + 0.00113001\mathrm{z})\mathrm{z}), \text{if } \mathrm{z}\epsilon\left[\frac{79}{80}, \frac{80}{80}\right] \end{cases}$$

Table 7. Approximate, exact solutions and error norms obtained for different fractional order of Example 3 at $\boldsymbol{T = 0.1, M = 80, \Delta\mathrm{r} = 0.0005}$.

x	$\alpha = 0.25$	$\alpha = 0.5$	$\alpha = 0.75$	$Exact\ Solution$
0.0	0.01	0.01	0.01	0.01
0.1	0.00950695	0.00950607	0.00950527	0.00951057
0.2	0.00808467	0.00808351	0.00808252	0.00809017
0.3	0.00587256	0.00587156	0.00587074	0.00587785

x	$\alpha = 0.25$	$\alpha = 0.5$	$\alpha = 0.75$	*Exact Solution*
0.4	0.00308696	0.0030864	0.00308595	0.00309017
0.5	0.0000000	0.0000000	0.0000000	0.0000000
0.6	−0.00308696	−0.0030864	−0.00308595	−0.00309017
0.7	−0.00587256	−0.00587156	−0.00587074	−0.00587785
0.8	−0.00808467	−0.00808351	−0.00808252	−0.00809017
0.9	−0.00950695	−0.00950607	−0.00950527	−0.00951057
1.0	−0.01	−0.01	−0.01	−0.01
$\mathfrak{L}_2$	4.04125×10^{-6}	4.86964×10^{-6}	5.56789×10^{-6}	
$\mathfrak{L}_\infty$	5.6717×10^{-6}	6.81543×10^{-6}	7.77594×10^{-6}	

Table 8. Error norms for $\alpha = 0.9$ of Example 3.

$M = 210, \Delta r = 0.0025$			$M = 130, \Delta r = 0.004$	
„T	$\mathfrak{L}_2$	$\mathfrak{L}_\infty$	$\mathfrak{L}_2$	$\mathfrak{L}_\infty$
0.2	4.7139×10^{-5}	6.61934×10^{-5}	5.48066×10^{-5}	7.68369×10^{-5}
0.4	6.12142×10^{-4}	8.65047×10^{-4}	6.21201×10^{-4}	8.77466×10^{-4}
0.6	3.20266×10^{-3}	4.52814×10^{-3}	3.21227×10^{-3}	4.54066×10^{-3}
0.8	1.03877×10^{-2}	1.46882×10^{-2}	1.03974×10^{-2}	1.4699×10^{-2}
1.0	2.58113×10^{-2}	3.64979×10^{-2}	2.58206×10^{-2}	3.65043×10^{-2}

Table 9. Error norms and numerical solutions of Example 3 when $T = 0.05, M = 100$ and $\alpha = 0.50$.

z	$\Delta r = 0.0005$	$\Delta r = 0.00025$	$\Delta r = 0.000125$	$\Delta r = 0.000625$	*Exact Solution*
0.0	0.0025	0.0025	0.0025	0.0025	0.0025
0.1	0.00237582	0.00237666	0.00237709	0.0023773	0.00237764
0.2	0.00202003	0.00202117	0.00202176	0.00202205	0.00202254
0.3	0.0014672	0.00146822	0.00146874	0.00146901	0.00146946
0.4	0.000771228	0.000771819	0.000772119	0.000772271	0.000772542
0.5	−0.0000000	−0.0000000	−0.0000000	−0.0000000	−0.0000000
0.6	−0.000771228	−0.000771819	−0.000772119	−0.000772271	−0.000772542
0.7	−0.0014672	−0.00146822	−0.00146874	−0.00146901	−0.00146946
0.8	−0.00202003	−0.00202117	−0.00202176	−0.00202205	−0.00202254
0.9	−0.00237582	−0.00237666	−0.00237709	−0.0023773	−0.00237764
1.0	−0.0025	−0.0025	−0.0025	−0.0025	−0.0025
$\mathfrak{L}_2$	1.81608×10^{-6}	9.89414×10^{-7}	5.69318×10^{-7}	3.56913×10^{-7}	
$\mathfrak{L}_2$	2.53291×10^{-6}	1.38005×10^{-6}	7.94403×10^{-7}	4.98851×10^{-7}	

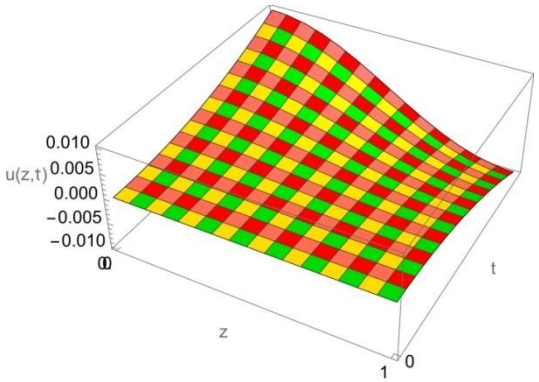

Figure 6. A 3D graphical depiction of the exact solutions for Example 3 is provided, using the values $M = 100, \Delta r = 0.01$ and $\alpha = 0.50$.

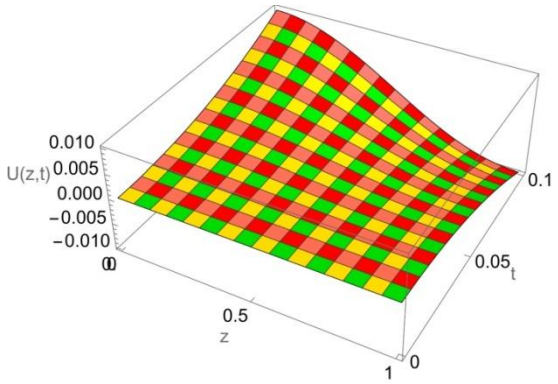

Figure 7. A 3D graphical depiction of the computational solutions for Example 3 is provided, using the values $M = 100, \Delta r = 0.01$ and $\alpha = 0.50$.

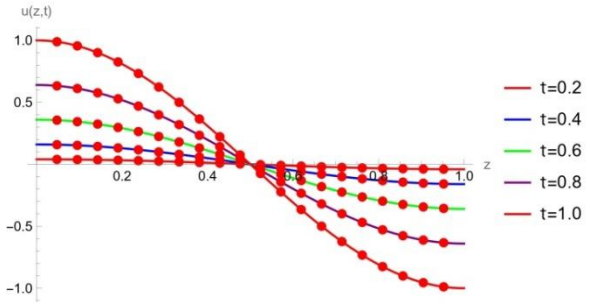

Figure 8. Numerical and exact results are plotted for $M = 100, \Delta x = 0.01$ and $\alpha = 0.50$, showcasing their behavior at different time levels.

5. CONCLUSIONS

- A Galerkin finite element method has been developed to numerically solve the time-fractional Burgers' equation.
- Cubic B-splines have been utilized for both trial and weight functions in the Galerkin finite element method, ensuring a flexible and accurate approximation of the solution.
- We accomplish the transition from the local to the global coordinate system by using a local-to-global transformation.
- The Caputo fractional derivative has been adopted to represent the fractional derivative in the governing equation. Discretization of this fractional term has been carried out using the L1 formula within the explicit finite difference method.
- The Crank-Nicolson method has been employed for the discretization of both the unknown functions and their spatial derivatives.
- The stability of the scheme has been thoroughly analyzed from a theoretical standpoint. To assess the efficiency and effectiveness of the proposed method, three numerical experiments involving problems with known exact solutions have been conducted.
- A detailed comparison has been conducted, contrasting the numerical results of the present study with those produced by the methodology presented in [19].
- The proposed scheme's performance and computational efficiency are visually depicted through graphical comparisons.
- The method's effectiveness for this specific class of time-fractional PDEs, along with its broader applicability to other time-fractional models, has been demonstrated by the findings.

REFERENCES

[1] Bhrawy, A. H., Zaky, M. A., Baleanu, D., *Romanian Reports in Physics*, **67**, 340, 2015.
[2] Cole, J. D., *Quarterly of Applied Mathematics*, **9**, 225, 1951.
[3] Chen, L., Lyu, S., Xu, T., *Applied Numerical Mathematics*, **169**, 164, 2021.
[4] Li, L., Li, D., *Applied Mathematics Letters*, **100**, 106011, 2020.
[5] Sugimoto, N., *Nonlinear Wave Motion*, **1**, 162, 1989.
[6] Safari, F., Chen, W., *Computers and Mathematics with Applications*, **96**, 55, 2021.
[7] Majeed, A., Kamran, M., Rafique, M., *Computers and Mathematics with Applications*, **39**, 257, 2020.
[8] Iqbal, M. K., Abbas, M., Nazir, T., Ali, N., *Advances in Difference Equations*, **2020**, 1, 2020.

[9] Esen, A., Tasbozan, O., *Acta Universitatis Sapientiae*, **7**, 167, 2015.
[10] Hassani, H., Naraghirad, E., *Mathematics and Computers in Simulation*, **162**, 1, 2019.
[11] Yadav, S., Pandey, R. K., *Chaos, Solitons and Fractals*, **133**, 109630, 2020.
[12] Li, C., Li, D., Wang, Z., *Mathematics and Computers in Simulation*, **187**, 357, 2021.
[13] Liu, J., Hou, G., *Applied Mathematics and Computation*, **217**, 7001, 2011.
[14] Yoku, A., Kaya, D., *Journal of Nonlinear Science and Applications*, **10**, 2017.
[15] Bec, J., Khanin, K., *Physics Reports*, **447**, 1, 2007.
[16] Ahmed, H. F., Bahgat, M. S. M., Zaki, M., *Pramana Journal of Physics*, **94**, 99, 2020.
[17] Zayernouri, M., Karniadakis, G. E., *SIAM Journal on Scientific Computing*, **36**, A40, 2014.
[18] Hussain, M., Haq, S., Ghafoor, A., Ali, I., *Computational and Applied Mathematics*, **39**, 6, 2020.
[19] Al-Saedi, A. A., Rashidinia, J., *Electronic Research Archive*, **31**, 4248, 2023.
[20] Momani, S., *Chaos Solitons and Fractals*, **28**, 930, 2006.
[21] Alsaedi A., Kirane, M., Torebek, B. T., *Quaestiones Mathematicae*, **43**, 185, 2020.
[22] Noureen, R., Iqbal, M. K., Asgir, M., Almohsen, B., Azeem, M., *Alexandria Engineering Journal*, ***116***, 451, 2025.
[23] Doha, E. H., Bhrawy, A. H., Abdelkawy, M. A., Hafez, R. M., *Central European Journal of Physics*, **12**, 111, 2014.
[24] Yaseen, M., Abbas, M., *International Journal of Computer Mathematics*, **97**, 725, 2020.
[25] Ben-Naim, E., Chen, S. Y., Doolen, G. D., Redner, S., *Physical Review Letters*, **83**, 4069, 1999.
[26] Shafiq, M., Abbas, M., Abdullah, F. A., Majeed, A., Abdeljawad, T., Alqudah, M. A., *Results in Physics*, **34**, 105244, 2022.
[27] El-Danaf, T. S., Hadhoud, A. R., *Applied Mathematical Modelling*, **36**, 4557, 2012.
[28] Akram, T., Abbas, M., Riaz, M. B., Ismail, A. I., Ali, N. M., *Alexandria Engineering Journal*, **59**, 2201, 2020.
[29] Onal, M., Esen, A., *Applied Mathematics and Nonlinear Sciences*, **5**, 177, 2020.
[30] Zayernouri, M., Karniadakis, G. E., *Journal of Computational Physics*, **293**, 312, 2015.